Journal of Engineering Mathematics **42:** 45–64, 2002.

Mass-transport enhancement in regions bounded by rigid walls

PHILIP M.J. TREVELYAN[1,3], SERAFIM KALLIADASIS[1,*], JOHN H. MERKIN[2] and STEPHEN K. SCOTT[3]
[1]*Department of Chemical Engineering, University of Leeds, Leeds, LS2 9JT, UK*
[2]*Department of Applied Mathematics, University of Leeds, Leeds, LS2, 9JT, UK*
[3]*School of Chemistry, University of Leeds, Leeds, LS2 9JT, UK*

Received 23 March 2001; accepted in revised form 8 October 2001

Abstract. The mass transport into a fluid bounded by stationary rigid walls in the limit of large Péclet number, Pe, is examined analytically. Two model systems are considered in detail: a stationary cavity and a model involving two concentric rotating cylinders. A macroscopic gradient is imposed between the top and bottom surfaces. It is demonstrated that mass transport into the fluid is enhanced owing to a recirculation zone which is connected to the solid boundary through a boundary layer of thickness $O(\mathrm{Pe}^{-1/3})$ in which cross-stream molecular diffusion is balanced by convection. The associated enhancement is large and scales as $\mathrm{Pe}^{1/3}$. Our asymptotic analysis is found to be in good agreement with numerical solutions of the full transport equation.

Key words: mass-transport enhancement, diffusion, effective diffusivity, recirculation zone.

1. Introduction

Engineering applications of interfacial mass transport can be found in a large variety of industrial processes and devices such as evaporators, heat exchangers, absorbers, scrubbers and falling film reactors. In several of these applications, mass is transported through unidirectional flow fields. However, diffusion can be significantly enhanced even when a small convective flow is generated in a direction normal to the originally parallel flow. For example, mass transport across a laminar falling film can increase by as much as a factor of 10 when waves appear at the interface [1] owing to the presence of a recirculation zone within the solitary waves that dominate the large-time evolution of the surface of the film [2]. Similarly, heat transport in a prototype system of two-dimensional flow between counter-rotating eccentric cylinders [3,4,5,6] has been shown to increase significantly (by orders of magnitude) when recirculation zones exist within the flow. We also note that flow fields with recirculation regions have been used successfully for separation purposes. For example, Baier *et al.* [7] suggested recently that the Taylor vortices in a Couette device can be used to enhance mass transport in separation processes significantly. Hence, flow-assisted diffusion has a profound impact on a large variety of mass/heat-transport applications and understanding the enhancement mechanism is crucial for the development of improved transport and separation processes.

This paper addresses the problem of mass-transport enhancement in confined regions bounded by rigid walls by considering the two specific cases of two-dimensional flow of a viscous incompressible fluid in a square cavity and the flow between two concentric cylinders as model systems. (We shall focus on mass transport subsequently. The analogy to heat transport is obvious.) Figures 1a and 5a sketch these two systems. The fluid motion in the cavity is

*Author to whom correspondence should be addressed. E-mail: S.Kalliadasis@leeds.ac.uk

generated by a steady disturbance – for example a small cylinder or a stirring device at the centre of the cavity – while the flow field between the two concentric cylinders is induced by the steady rotation of the inner cylinder in its own plane. Both problems are of intrinsic theoretical importance as they represent simple examples of steady flows involving closed streamlines and they are part of the larger class of steady separated flows. Both the flow and concentration fields are assumed to be steady; time-dependent modulations of the flow field can lead to chaotic advection which is beyond the scope of the present paper. Of particular interest is the case where advection dominates over diffusion. The relative importance of advection and diffusion in the transport process is measured by the Péclet number, Pe, and hence we are interested in the distinguished limit of large Pe – it should be noted that mass-transport devices necessarily operate at extremely high Péclet numbers.

The associated problem of mass-transport in a driven cavity was recently considered by the authors [8]. The study was a systematic parametric investigation of mass-transport enhancement in a driven square cavity with and without a chemical reaction and for a wide range of Reynolds and Péclet numbers and dimensionless reaction-rate constants. It was demonstrated that, in the absence of a chemical reaction, the primary mechanism for mass-transport enhancement is a large recirculation zone present almost everywhere in the cavity, except very close to the walls where molecular diffusion balances convection in thin boundary layers.

The same mechanism is present in the prototypes shown in Figures 1a and 5a: for large Pe, the enhancement over pure diffusion mass-transport without recirculation will be much more pronounced. In this case, the circuit time of the circulation in the cavity and cylinder models is much shorter than the diffusive time scale and in steady-state mixing along each streamline effectively removes concentration gradients. As a result, the cross-stream advection due to the recirculation is far more important than diffusion and the recirculation zone becomes a well-mixed region at steady-state (this effectively reduces the distance for diffusive transport).

Although mass/heat transport by buoyancy-induced convective motions in enclosed rectangular cavities has been investigated by several authors (see for instance Patterson and Imberger [9]), previous analyses of steady high-Péclet-number transport in regions with closed streamlines have been restricted mainly to mobile interfaces: for example Shraiman [10], Polyanin [11], Young *et al.* [12] and Rosenbluth *et al.* [13] examined in detail the transport process between recirculation cells. Since the transport in this system is effectively between two well-mixed convective cells, the enhancement is determined by a diffusive boundary layer of thickness $\mathrm{Pe}^{-1/2}$ at the boundary of the two cells (the boundary in this case is a separatrix connecting stagnation points and the diffusive layer is similar to the boundary layer near mobile interfaces with a thickness that varies as $\mathrm{Pe}^{-1/2}$; see the review by Stewart [14]). Consequently, the effective transport enhancement (or *effective diffusivity*) across circulation cells varies as $\mathrm{Pe}^{1/2}$. When the top and bottom boundaries of the convection rolls are replaced with rigid walls, Shraiman [10], Young *et al.* [12] and Rosenbluth *et al.* [13] argued that diffusion is not effective during the turn of the mobile boundary layer onto the rigid wall and hence the concentration simply follows the streamlines around the corner: the variation of the concentration field along the streamlines adjacent to solid boundaries can be neglected. Consequently, the effective diffusivity is, to leading order, the diffusivity computed by assuming that all interfaces are mobile. This greatly simplifies the analysis which could otherwise involve matching boundary layers of different thickness.

For the stationary cavity problem considered here, we will be interested mainly in developing an analytical method of solution. The problem of computing mass-transport through laminar boundary layers is, in general, a difficult one because of the complicated nature of

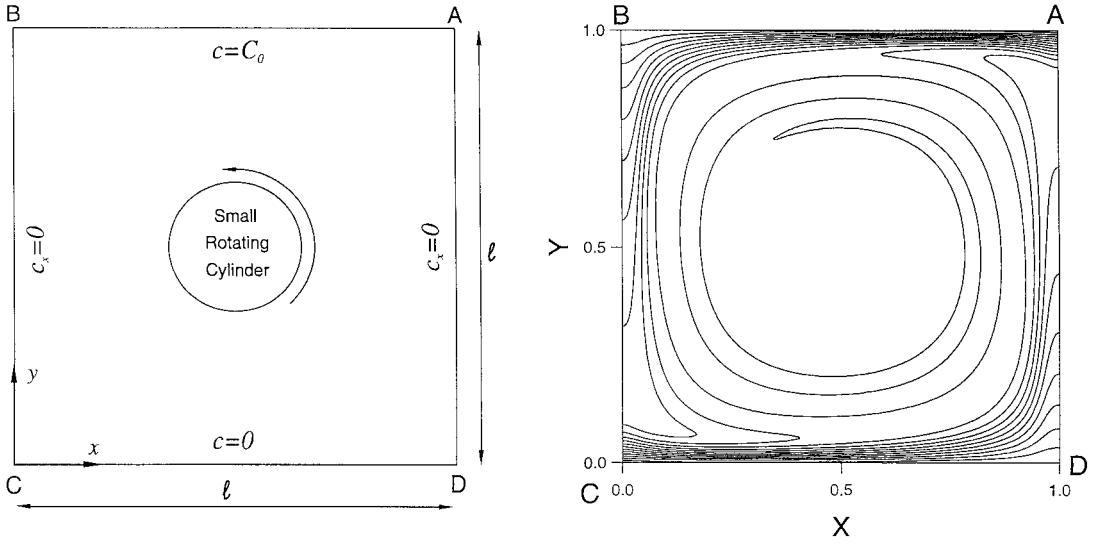

Figure 1. (a) Sketch of the rectangular-cavity-model problem. The flow is in the counterclockwise direction and is induced by a disturbance at the center; (b) concentration contours in the stationary cavity obtained from a numerical solution of the full transport equation for $\mathrm{Pe} = 10^3$.

the governing equations and possible variations in the thickness of the boundary layer. For the stationary cavity problem, we shall demonstrate that an analytical solution is possible as the diffusive boundary layers on all four stationary walls are of the same thickness, $\mathrm{Pe}^{-1/3}$ (see, for instance, Acrivos and Goddard [15] for the problem of laminar flow over a semi-infinite flat plate). It will be shown that all four boundary layers connect to a region where the concentration is spatially homogeneous. We shall examine the transport mechanism in detail through the analytical solutions, valid for $\mathrm{Pe} \gg 1$, for the concentration fields derived for both the cavity and the cylinder models. The enhancement of the flux across the top surface over pure diffusion without recirculation will be shown to vary as $\mathrm{Pe}^{1/3}$, as simple scaling arguments demonstrate. For the diffusion problem in a Rayleigh–Bénard convection cell, Shraiman [10] obtained analytically the concentration field using matched asymptotic expansions. We shall utilise here some of his asymptotic concepts to resolve the diffusive boundary layers which bound our recirculation zone in order to obtain the effective diffusivity and hence the average flux across the top surface. Notice that, in our case, there is a flux of concentration at the top surface of the cavity which qualitatively changes the mechanism for spreading the concentration.

2. Stationary cavity

We consider the steady, planar, laminar motion of an incompressible, constant-viscosity, Newtonian fluid in a square cavity of characteristic dimension ℓ. The flow in the cavity can, for example, be induced by the steady rotation of a small cylinder located at the centre of the cavity, as illustrated in Figure 1a. We define $\hat{\psi} = 0$ on the cavity boundary, while the flow is driven in an anti-clockwise motion. To facilitate the analysis we take, for simplicity, a given flow field

$$\hat{\psi} = 256\ell^{-7}U_0x^2(\ell - x)^2y^2(\ell - y)^2, \tag{1}$$

in terms of the orthogonal coordinate system (x, y) whose origin is placed at the left corner of the bottom wall. This stream function makes an analytical approach to the problem possible, though still providing a recirculation zone.

We now introduce a passive species into the cavity via the top surface such that the concentration there assumes the prescribed surface value $c = C_0$ at $y = \ell$. We also impose a macroscopic gradient, by which the absorbed species is removed completely from the system through the bottom surface at $y = 0$ via a perfect surface catalyst (alternatively we could achieve the same effect by assuming that a porous medium is present at $y = 0$), and hence $c = 0$ at $y = 0$. The two vertical walls are assumed to be impermeable and so no-flux boundary conditions are imposed there with $c_x = 0$ at $x = 0$ and $x = \ell$.

The appropriate equation for the steady-state mass-transport of the absorbed species is

$$(\mathbf{u} \cdot \nabla)c = D\nabla^2 c$$

with D the molecular diffusivity. We now introduce the non-dimensionalisation, $c = C_0 C$, $x = \ell X$, $y = \ell Y$ and $\hat{\psi} = \ell U_0 \psi$ to obtain the dimensionless governing equation for the concentration field

$$\mathrm{Pe}(\psi_Y C_X - \psi_X C_Y) = C_{XX} + C_{YY}, \tag{2a}$$

where $\mathrm{Pe} = U_0 \ell / D$ is the Péclet number which expresses the relative importance of convection over diffusion. The associated boundary conditions are

$$C_X = 0 \quad \text{at} \quad X = 0 \quad \text{and} \quad X = 1 \quad (0 < Y < 1), \tag{2b}$$

$$C = 1 \quad \text{at} \quad Y = 1 \qquad (0 < X < 1), \tag{2c}$$

$$C = 0 \quad \text{at} \quad Y = 0 \qquad (0 < X < 1). \tag{2d}$$

As was pointed out in the Introduction, in the high-Pe limit the steady cross-stream convection associated with the recirculation zone dominates over diffusion. In this limit, the outer region (the term 'outer' here refers to the recirculation zone away from the boundaries) of Equation (2a) is described by the equation

$$-\psi_Y C_X + \psi_X C_Y = 0 \tag{3}$$

and hence the streamlines are identical to the concentration contours, so that $C = C(\psi)$ to leading order. This simply means that the concentration along each streamline is constant due to the strong advection mixing. However, this may or may not lead to a constant-concentration outer region. To show that this is the case, consider an arbitrary closed streamline Γ with corresponding stream function ψ_0. After invoking the divergence theorem and the continuity equation $\nabla \cdot \mathbf{u} = 0$, we obtain

$$\oint_\Gamma \hat{\eta} \cdot (\nabla C) \mathrm{d}s = 0 \tag{4}$$

with $\hat{\eta}$ the (outward) unit normal along Γ. This simply means that at steady state there is no accumulation and no convection across Γ and the total diffusive flux must vanish exactly. We now have, $\nabla C = (\mathrm{d}C/\mathrm{d}\psi)\nabla\psi$ from $C = C(\psi)$ and hence

$$\oint_\Gamma (\nabla C) \cdot \hat{\eta} \mathrm{d}s = \frac{\mathrm{d}C}{\mathrm{d}\psi}(\psi_0) \oint_\Gamma \hat{\eta} \cdot \nabla\psi \mathrm{d}s = 0 \tag{5}$$

and since $\hat{\eta} = \nabla\psi/|\nabla\psi|$ the line integral $\oint_\Gamma \hat{\eta}\cdot\nabla\psi \mathrm{d}s$ is simply $\oint_\Gamma |\nabla\psi|\mathrm{d}s$ which is non-zero. Consequently,

$$\frac{\mathrm{d}C}{\mathrm{d}\psi}(\psi_0) = 0 \tag{6}$$

and since ψ_0 can be any closed streamline, Equation (6) then implies that the concentration is, to leading order, homogeneous in the outer region.

2.1. Boundary-layer analysis, $\mathrm{Pe} \gg 1$

The full problem consists of an elliptic equation, Equation (2), in a finite region with boundary conditions on all four walls, whose numerical solution for $\mathrm{Pe} = 10^3$ is shown in Figure 1b. However, by introducing appropriate boundary-layer coordinates, we may convert the problem into two parabolic equations, each defined over an infinite region. We shall obtain the full solution by appropriately matching the solutions of the two parabolic equations with the constant-concentration outer solution and by imposing a global self-consistency condition.

In the regions close to the stationary walls, there exists a boundary layer whose thickness can be easily determined when we consider the dominant terms there. Let us take, for example, the top wall: as $Y \to 1$ we have $\psi_X = O((1-Y)^2)$, $\psi_Y = O(1-Y)$, $C_X = O(1)$, $C_{XX} = O(1)$, $C_Y = O((1-Y)^{-1})$, $C_{YY} = O((1-Y)^{-2})$ and hence $\mathrm{Pe}(\psi_Y C_X - \psi_X C_Y) = O(\mathrm{Pe}(1-Y))$. Therefore, we can consider the following possibilities: $\mathrm{Pe}(1-Y)^3 \ll (1-Y)^2$, $\mathrm{Pe}(1-Y)^3 \ll 1$, $\mathrm{Pe}(1-Y)^3 \sim (1-Y)^2$, $1 \ll \mathrm{Pe}(1-Y)^3$ and $\mathrm{Pe}(1-Y)^3 \sim 1$. In the first three cases we may approximate Equation (2a) with $C_{Y_{\mathrm{in}}Y_{\mathrm{in}}} = 0$, where Y_{in} is the inner coordinate, which yields a linear concentration profile in the boundary layer that satisfies the boundary condition (2c) but it cannot match the outer solution. The fourth possibility yields, $\psi_{Y_{\mathrm{in}}} C_X - \psi_X C_{Y_{\mathrm{in}}} = 0$ with general solution $C = C(\psi)$ to leading order in the boundary layer region (see discussion in Section 2). We let $f_{AB}(\psi)$ denote the AB boundary layer solution that satisfies the wall boundary condition and matches the outer region (we note that this does not uniquely define f_{AB}). However, matching of the boundary layers AB and BC in the neighbourhood of corner B indicates that $f_{AB}(\psi) = f_{BC}(\psi)$. Similarly $f_{BC}(\psi) = f_{CD}(\psi)$ and hence $f_{AB}(\psi) = f_{CD}(\psi)$. But, $f_{AB}(0) = 1$ and $f_{CD}(0) = 0$ as $\psi = 0$ on the solid boundary and the boundary layer solutions must satisfy the top and bottom wall boundary conditions. This obviously leads to a contradiction and hence we are left with the final possibility, the distinguished limit $(1-Y) = O(\mathrm{Pe}^{-1/3})$. Physically, this means that molecular diffusion across the boundary layer is balanced by advection there. Hence, the concentration across the top boundary-layer region varies with $\mathrm{Pe}^{1/3}(1-Y)$ (in terms of dimensional variables, the size of the boundary layer is $\ell_b \sim \mathrm{Pe}^{-1/3}\ell$). A similar argument shows that a concentration boundary layer of thickness $\delta \sim \mathrm{Pe}^{-1/3}$ is present near all four stationary walls.

We now introduce the boundary-layer coordinates, τ, which is almost tangential to the streamlines, and σ, a cross-streamline coordinate. For convenience, we set $A(\zeta) = 256\zeta^2(1-\zeta)^2$, such that the σ and τ coordinates are in general defined from a modified *Von Mises* transformation

$$\sigma = \left(\frac{3\mathrm{Pe}}{4}\right)^{1/3}\psi^{\frac{1}{2}} \quad \text{and} \quad \tau = \frac{1}{a_o^2}\int_0^\lambda \sqrt{A(\zeta)}\mathrm{d}\zeta, \tag{7}$$

where

$$a_o^2 = \int_0^1 \sqrt{A(\zeta)}\mathrm{d}\zeta = 8/3, \quad \lambda = \frac{1}{2} + \frac{n}{2}\left(\frac{Y-\frac{1}{2}}{X-\frac{1}{2}}\right)^n$$

and $n = \text{sign}(A(Y) - A(X))$, such that both σ and τ are $O(1)$ in the boundary layer. Notice that $n > 0$ for the vertical boundaries and $n < 0$ for the horizontal boundaries. Also, both λ and τ increase in the direction of flow, and are defined so that $\lambda, \tau \in [0, 1]$. Although λ, and hence τ, depend on both X and Y, especially in the neighbourhood of the corners, near the boundaries the dependence on the coordinate perpendicular to the boundary is much weaker. We also note that near AB, $\lambda \simeq 1 - X$, near BC, $\lambda \simeq 1 - Y$, near CD, $\lambda \simeq X$ and near DA, $\lambda \simeq Y$, with the corners A, B, C and D as indicated in Figure 1a. For our problem, we take

$$\sigma = \left(\frac{3\text{Pe}}{4}\right)^{1/3} 16XY(1-Y)(1-X) \quad \text{and} \quad \tau = 3\lambda^2 - 2\lambda^3. \tag{8}$$

For example, near the top horizontal wall AB, we have $1-Y \ll 1$, – in fact $1-Y = O(\text{Pe}^{-1/3})$ – and hence, $\psi \simeq A(X)(1-Y)^2$ with $\psi = O(\text{Pe}^{-2/3})$. Therefore, for the top boundary,

$$\sigma \simeq \left(\frac{3Pe}{4}\right)^{1/3} 16X(1-X)(1-Y) \quad \text{and} \quad \tau \simeq 1 + 2X^3 - 3X^2.$$

Substituting these transformations in Equation (2a), the mass-transport equation for C^{AB}, the concentration near AB, is

$$\begin{aligned}\text{Pe}(\psi_Y\tau_X - \psi_X\tau_Y)C^{AB}_\tau \;=\; &\left(\frac{3\text{Pe}}{4}\right)^{2/3} |\nabla\psi^{\frac{1}{2}}|^2 C^{AB}_{\sigma\sigma} + \left(\frac{3\text{Pe}}{4}\right)^{1/3} (\nabla^2\psi^{\frac{1}{2}})C^{AB}_\sigma \\ &+ 2\left(\frac{3\text{Pe}}{4}\right)^{1/3} (\nabla\psi^{\frac{1}{2}}\cdot\nabla\tau)C^{AB}_{\sigma\tau} + (\nabla^2\tau)C^{AB}_\tau + |\nabla\tau|^2 C^{AB}_{\tau\tau}.\end{aligned}$$

The first and second terms on the left-hand side of the above equation are of $O(\text{Pe}^{2/3})$ and $O(\text{Pe}^{1/3})$, respectively, while the first term on the right-hand side is of $O(\text{Pe}^{2/3})$ with the remaining terms being of $O(\text{Pe}^{1/3})$. Thus, retaining only the leading order terms yields

$$4\tau_X C^{AB}_\tau = \left(\frac{3}{4}\right)^{2/3} \text{Pe}^{-1/3}\psi_Y\psi^{-1}C^{AB}_{\sigma\sigma} + O(\text{Pe}^{-2/3}) \tag{9}$$

which can be rewritten as

$$C^{AB}_\tau = \sigma^{-1}C^{AB}_{\sigma\sigma}. \tag{10}$$

Similarly we find that for the left vertical wall BC with boundary-layer coordinates

$$\sigma \simeq \left(\frac{3\text{Pe}}{4}\right)^{1/3} 16XY(1-Y) \quad \text{and} \quad \tau \simeq 1 + 2Y^3 - 3Y^2,$$

the boundary-layer concentration equation is given by Equation (10), with C^{AB} replaced by C^{BC}.

We now demonstrate that the concentration in the outer region is exactly $1/2$: with $C(X, Y)$ denoting the solution of (2), $C(1-X, 1-Y)$ would be the solution for the concentration field in a cavity rotated 180° with $C = 0$ and $C = 1$ at the top and bottom walls, respectively, maintaining the flow in an anti-clockwise motion. Consider now a cavity with $C = 1$ at both the top and bottom surfaces. The solution in this case is trivial, *i.e.* $C = 1$ everywhere. This problem is simply a superposition of the two previous problems with solutions $C(X, Y)$ and

$C(1-X, 1-Y)$ (due to the linearity of the transport equation; notice also that the coefficients of the equation depend on ψ which is always the same) and hence $C(X, Y)+ C(1 - X, 1 - Y) = 1$. In terms of the (σ, τ) coordinates we have $C(\sigma, \tau) + C(\sigma, 1 + \tau) = 1$ and since both $C(\sigma, \tau)$ and $C(\sigma, 1 + \tau)$ approach the constant concentration in the outer region as $\sigma \to \infty -$ this signifies matching with the regular solution in the spatially homogeneous outer region – the concentration in the outer region must be $1/2$. Therefore, only the solution near any two adjacent walls is required, as the sum of concentrations near A or C equals 1, for any value of σ. Hence, on the horizontal wall AB, the following boundary conditions must be satisfied by the inner region:

$$C = s(\sigma) \quad \text{at} \quad \tau = 0, \quad C \to \tfrac{1}{2} \quad \text{as} \quad \sigma \to \infty \quad \text{and} \quad C = 1 \quad \text{at} \quad \sigma = 0, \tag{11}$$

where the function $s(\sigma)$, the concentration C on $\tau = 0$, is an, as yet, unknown function which we shall determine using a global self-consistency condition.

Similarly, on the vertical wall BC, the boundary conditions to be satisfied by the inner region are,

$$C = t(\sigma) \quad \text{at} \quad \tau = 0, \quad C \to \tfrac{1}{2} \quad \text{as} \quad \sigma \to \infty \quad \text{and} \quad C_\sigma = 0 \quad \text{at} \quad \sigma = 0, \tag{12}$$

where the function $t(\sigma)$, the concentration C on $\tau = 0$, will be obtained from the solution on the wall AB.

2.2. Solution for the inner region

We introduce $\overline{C}$ and $\hat{C}$, both satisfying Equation (10) but with the following boundary conditions

$$\overline{C} = \tfrac{1}{2} \quad \text{and} \quad \hat{C} = s(\sigma) - \tfrac{1}{2} \quad \text{on} \quad \tau = 0,$$

$$\overline{C} \to \tfrac{1}{2} \quad \text{and} \quad \hat{C} \to 0 \quad \text{as} \quad \sigma \to \infty,$$

$$\overline{C} = 1 \quad \text{and} \quad \hat{C} = 0 \quad \text{on} \quad \sigma = 0,$$

so that $\overline{C}+\hat{C}$ satisfies the boundary conditions in (11), with $\hat{C}$ satisfying homogeneous boundary conditions. The equation for $\overline{C}$ can now be reduced to an ordinary differential equation with respect to the single variable $\eta = \sigma/\tau^{1/3}$ and hence $\overline{C}$ is self-similar. A first integral of the resulting equation can be readily obtained, $\overline{C}_\eta \sim \mathrm{e}^{-\eta^3/9}$, which after using the boundary conditions gives:

$$\overline{C} = 1 - \frac{3^{\frac{1}{3}}}{2\Gamma(\frac{1}{3})} \int_0^{\sigma/\tau^{\frac{1}{3}}} \mathrm{e}^{-z^3/9}\, \mathrm{d}z. \tag{13}$$

To find $\hat{C}$ we first take the Airy transform of Equation (10) (see Appendix 1), defined from $U(z, \tau) = \frac{\sqrt{3}}{2} \int_0^\infty \hat{C}(\sigma, \tau)\sigma G(-\sigma z)\mathrm{d}\sigma$ where $G(z) = -\sqrt{3}\mathrm{Ai}(z) + \mathrm{Bi}(z)$, and $\mathrm{Ai}(z)$ and $\mathrm{Bi}(z)$ are Airy functions [16, pp. 446–450], to obtain:

$$U_\tau(z, \tau) = \frac{\sqrt{3}}{2} \int_0^\infty \hat{C}_{\sigma\sigma}(\sigma, \tau) G(-\sigma z)\mathrm{d}\sigma = \frac{\sqrt{3}}{2} \int_0^\infty \hat{C}(\sigma, \tau) G_{\sigma\sigma}(-\sigma z)\mathrm{d}\sigma.$$

Using the result that $G_{\sigma\sigma}(-\sigma z) = -z^3\sigma G(-\sigma z)$, we then have $U_\tau(z,\tau) = -z^3 U(z,\tau)$, with solution $U(z,\tau) = U(z,0)\mathrm{e}^{-z^3\tau}$, where $U(z,0) = \frac{\sqrt{3}}{2}\int_0^\infty \left(s(p) - \frac{1}{2}\right) pG(-pz)\mathrm{d}p$. Taking the inverse transform, we obtain

$$\hat{C} = \frac{3}{4}\int_0^\infty z\mathrm{e}^{-z^3\tau} G(-z\sigma)\int_0^\infty \left(s(p) - \frac{1}{2}\right) pG(-zp)\mathrm{d}p\,\mathrm{d}z, \tag{14}$$

and the concentration in the boundary layer near the top horizontal wall AB is given by

$$C = 1 - \frac{3^{\frac{1}{3}}}{2\Gamma(\frac{1}{3})}\int_0^{\sigma/\tau^{\frac{1}{3}}} \mathrm{e}^{-z^3/9}\mathrm{d}z + \frac{3}{4}\int_0^\infty z\mathrm{e}^{-z^3\tau} G(-z\sigma)\int_0^\infty \left(s(p) - \frac{1}{2}\right) pG(-zp)\mathrm{d}p\,\mathrm{d}z \tag{15}$$

The concentration profile near the corner B is obtained by letting $\tau \to 1$ in expression (15). This gives

$$t(\sigma) = 1 - H(\sigma) + \frac{3}{4}\int_0^\infty z\mathrm{e}^{-z^3} G(-z\sigma)\int_0^\infty \left(s(p) - \frac{1}{2}\right) pG(-zp)\mathrm{d}p\,\mathrm{d}z \tag{16}$$

where $H(\sigma) = \frac{3^{\frac{1}{3}}}{2\Gamma(\frac{1}{3})}\int_0^\sigma \mathrm{e}^{-z^3/9}\mathrm{d}z = \frac{1}{2}(1 - \Gamma(\frac{1}{3}, \frac{\sigma^3}{9})/\,\Gamma(\frac{1}{3}))$ with $\Gamma(a,x)$ the incomplete Gamma Function [16, pp. 260–263].

We now solve for the boundary layer near the wall BC. Again we introduce $\overline{C}$ and $\hat{C}$ both satisfying Equation (10) but with the following boundary conditions

$$\overline{C} = \tfrac{1}{2} \quad \text{and} \quad \hat{C} = t(\sigma) - \tfrac{1}{2} \quad \text{on} \quad \tau = 0,$$

$$\overline{C} \to \tfrac{1}{2} \quad \text{and} \quad \hat{C} \to 0 \quad \text{as} \quad \sigma \to \infty,$$

$$\overline{C}_\sigma = 0 \quad \text{and} \quad \hat{C}_\sigma = 0 \quad \text{on} \quad \sigma = 0,$$

so that $\overline{C} + \hat{C}$ satisfies the boundary conditions in (12), with $\hat{C}$ satisfying homogeneous boundary conditions. The solution for $\overline{C}$ is simply $\frac{1}{2}$. Notice that the boundary condition $C \to t(\sigma)$ as $\tau \to 0$ is the matching condition for the boundary layers AB and BC in the vicinity of corner B. Indeed, the $C = 1$ boundary condition on the wall AB and $C \to \frac{1}{2}$ away from the wall imply that molecular diffusion along the X direction can be neglected and hence the concentration contours in the AB boundary layer are, to leading order, straight lines parallel to the wall. In fact, as the boundary condition on the vertical wall just after corner B is $C_X = 0$, the concentration contours in the AB boundary layer do not change as the BC wall is approached and hence the solution for the top boundary layer is valid all the way to the corner, thus allowing matching with the vertical boundary layer. This observation is consistent with the numerical solution of the full transport Equation (2a) depicted in Figure 1b with $\mathrm{Pe} = 10^3$ and is similar to the idea of relating the inner solution just before the edges of a finite-length boundary layer to that immediately past these edges, introduced by Kuiken in his study of heat and mass-transport from an open cavity [17].

Following now an analysis similar to that for the wall AB, we can determine $\hat{C}$ using the Airy transform. The result is

$$\hat{C} = \frac{3}{4}\int_0^\infty z\mathrm{e}^{-z^3\tau}\overline{G}(-z\sigma)\int_0^\infty \left(t(p) - \tfrac{1}{2}\right) p\overline{G}(-zp)\mathrm{d}p\,\mathrm{d}z, \tag{17}$$

where $\overline{G}(z) = \sqrt{3}\mathrm{Ai}(z) + \mathrm{Bi}(z)$. Finally, the concentration in the boundary layer near the left vertical wall BC is given by

$$C = \frac{1}{2} + \frac{3}{4}\int_0^\infty z\mathrm{e}^{-z^3\tau}\overline{G}(-z\sigma)\int_0^\infty \left(t(p) - \tfrac{1}{2}\right) p\overline{G}(-zp)\mathrm{d}p\,\mathrm{d}z. \tag{18}$$

Again, if simple symmetry arguments are used, the inner solution near corner C is $1-s(\sigma)$, where

$$1 - s(\sigma) = \frac{1}{2} + \frac{3}{4}\int_0^\infty z\mathrm{e}^{-z^3}\overline{G}(-z\sigma)\int_0^\infty \left(t(p) - \tfrac{1}{2}\right) p\overline{G}(-zp)\mathrm{d}p\,\mathrm{d}z. \tag{19}$$

Therefore, using Equation (16) for $t(p)$, we get

$$\begin{aligned} s(\sigma) \;=\; & \frac{1}{2} - \frac{3}{4}\int_0^\infty z\mathrm{e}^{-z^3}\overline{G}(-z\sigma)\int_0^\infty p\overline{G}(-zp)\left(\tfrac{1}{2} - H(p)\right)\mathrm{d}p\,\mathrm{d}z \\ & - \frac{9}{16}\int_0^\infty z\mathrm{e}^{-z^3}\overline{G}(-z\sigma)\int_0^\infty p\overline{G}(-zp)\int_0^\infty q\mathrm{e}^{-q^3}G(-qp) \\ & \int_0^\infty \left(s(r) - \tfrac{1}{2}\right) rG(-rq)\mathrm{d}r\mathrm{d}q\mathrm{d}p\,\mathrm{d}z \end{aligned} \tag{20}$$

which is a global self-consistency condition. This integral equation for $s(\sigma)$ was solved numerically by approximating the kernel with a large finite matrix and inverting the resulting linear system. The domain size and step size were chosen so that larger regions with smaller step sizes produced graphically indistinguishable results. A domain size of 20 with uniform step sizes of 0·02 was found to provide sufficiently accurate results.

The function $t(\sigma)$ was then computed from Equation (16), see Figure 2. We notice that $t(\sigma) \to 1$ as $\sigma \to 0$ and $t(\sigma) \to 1/2$ as $\sigma \to \infty$. We see the classical undershoot around $\sigma = 2{\cdot}6$, which is followed by very rapidly decaying oscillations tending to a value of $1/2$ into the outer region (not visible in the graph).

Figure (3a) depicts the inner region concentration contours in (σ, τ) co-ordinates obtained from the boundary-layer analysis. Notice the excellent agreement with the numerical solution of the full transport Equation (2a) shown in Figure (3b) for $\mathrm{Pe} = 10^3$. The numerical solution was determined by use of a standard finite-difference method in the $x - y$ co-ordinates (*i.e.* solving Equations (2)), with the solution then mapped onto the $\sigma - \tau$ plane.

2.3. Effective diffusivity

The effective diffusivity can be estimated by observing that the average flux through the top wall is equal to the diffusive flux f through the boundary layer. This scales as $f \sim D/\ell_b \sim D/(\mathrm{Pe}^{-1/3}\ell)$, since c_y scales as $\Delta c/\ell_b$ with Δc of $O(1)$. We now set this flux equal to $f = -D_{\mathrm{eff}}\bar{c}_y$ with $\bar{c}$ the concentration field averaged locally over the top surface of the cavity. The mean concentration gradient is simply $\bar{c}_y \sim \Delta c/\ell$ so that $D_{\mathrm{eff}} \sim D\mathrm{Pe}^{1/3}$ which is a measure of the enhancement of the diffusivity for $\mathrm{Pe} \gg 1$. Alternatively, the flux without a boundary layer is simply $f_0 \sim D/\ell$ and the flux with a boundary layer is $f \sim D/\ell_b \sim D/(\mathrm{Pe}^{-1/3}\ell)$. The diffusive flux is hence enhanced: $f/f_0 \sim \mathrm{Pe}^{1/3}$ and $f/f_0 \sim D_{\mathrm{eff}}/D$ by definition, so that $D_{\mathrm{eff}}/D \sim \mathrm{Pe}^{1/3}$.

Our analysis of the previous section allows us to determine the coefficient in front of the $\mathrm{Pe}^{1/3}$ scaling. With f denoting the dimensional flux at the top surface,

$$f \;=\; -\frac{D}{\ell}\int_0^\ell c_y|_{y=\ell}\mathrm{d}x.$$

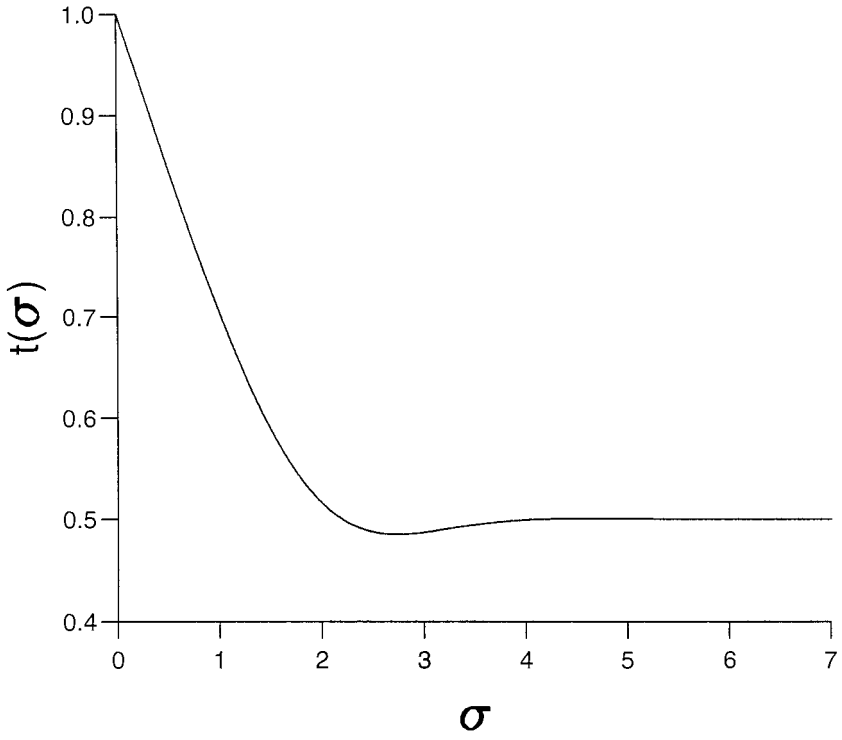

Figure 2. The concentration $t(\sigma)$, given by expression (16), near corner B.

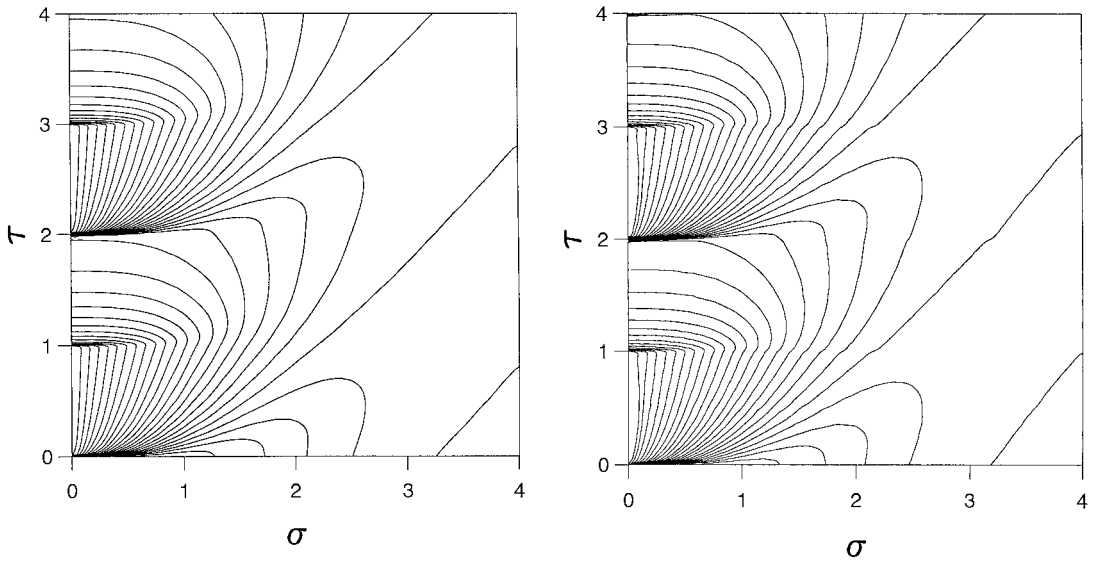

Figure 3. (a) Inner region concentration contours obtained from the boundary-layer solution; (b) Inner region concentration contours obtained numerically from the full transport equation $(2a)$ for $\mathrm{Pe} = 10^3$ and mapped onto the $\sigma - \tau$ plane.

The effective diffusivity can be defined as

$$D_{\text{eff}} = -\frac{f}{\overline{c}_y}$$

where $\overline{c}_y$ is the mean macroscopic gradient in the y direction, C_0/ℓ, which yields

$$D_{\text{eff}} = -\frac{f\ell}{C_0} = \frac{D}{C_0}\int_0^{\ell} c_y|_{y=\ell}\mathrm{d}x = D\int_0^1 C_Y|_{Y=1}\mathrm{d}X.$$

We then have $\int_0^1 C_Y|_{_{Y=1}}\mathrm{d}X = -\frac{8}{3}\,(3\mathrm{Pe}/4)^{1/3}\int_0^1 C_\sigma|_{_{\sigma=0}}\mathrm{d}\tau$, and from Equation (15), we obtain

$$\begin{aligned}\int_0^1 C_\sigma|_{_{\sigma=0}}\mathrm{d}\tau \;&=\; -\frac{3^{4/3}}{4\Gamma(\frac{1}{3})} - \frac{3^{7/6}}{2\Gamma(\frac{1}{3})}\int_0^\infty \frac{1}{z}(1-\mathrm{e}^{-z^3})\int_0^\infty \left(s(p)-\tfrac{1}{2}\right) pG(-zp)\mathrm{d}p\mathrm{d}z\\ &=\; -0{\cdot}4793.\end{aligned}$$

Hence,

$$D_{\text{eff}} = 1{\cdot}1613D\mathrm{Pe}^{1/3} \tag{21}$$

We notice that our solution applies to the problem of heat transport in a square cavity as well with D_{eff}/D equivalent to the (mean) Nusselt number in the heat transport case. In Figure 4 we give a plot D_{eff}/D from expression (21) (full line) as well as values obtained from numerical solution of (2a) for a range of Pe (shown by $\times$). The Figure shows excellent agreement between the results from our asymptotic analysis and the numerically determinated values. There is still agreement, even when Pe is $O(1)$, where our analysis is no longer valid. This suggests that expression (21) gives a reliable guide to the effective diffusivity D_{eff} for all values of Pe of practical interest.

We finally comment on the more general problem of a rectangular cavity of length ℓ_x and depth ℓ_y. In this case, we can map the rectangle into a square using $x = \ell_x X$, $y = \ell_y Y$ and $\hat{\psi} = 256\ell_x^{-4}\ell_y^{-3}U_0x^2(\ell_x-x)^2y^2(\ell_y-y)^2$ such that $\hat{\psi} = U_0\ell_y\psi$ with ψ identical to the square cavity case. The transport equation now becomes, $\mathrm{Pe}(\psi_Y C_X - \psi_X C_Y) = C_{XX} + (\ell_x/\ell_y)^2 C_{YY}$ where $\mathrm{Pe} = U_0\ell_y/D$. The inner coordinates σ and τ are the same as before (Equation (7)) with the inner equation for the vertical walls being identical to the square cavity case but for the horizontal walls the inner equation now reads $C_\tau = (\ell_x/\ell_y)^2 C_{\sigma\sigma}/\sigma$. The solution to this equation can be easily obtained by rescaling σ. We can then follow the same procedure used to derive the global self-consistency condition, Equation (20). The new condition has the same functional form with the square cavity case except that $\overline{G}(-z\sigma)$ is now replaced with $\overline{G}(-(\ell_y/\ell_x)^{2/3}z\sigma)$, $H(p)$ with $H((\ell_x/\ell_y)^{2/3}p)$ and $G(-qp)$ with $G(-(\ell_x/\ell_y)^{2/3}qp)$. Hence, for a rectangular cavity Equation (20) is parameterized by the aspect ratio ℓ_y/ℓ_x and will have to be solved numerically for different values of this ratio resulting in a coefficient different to 1·1613 in front of the scaling $D\mathrm{Pe}^{1/3}$ in (21) valid for a square cavity.

3. The concentric cylinders model

We now consider the steady, planar, laminar motion of an incompressible, constant-viscosity, Newtonian fluid between two concentric cylinders of radii a and b with $a > b$. The flow is induced by the steady rotation of the inner cylinder in its own plane such that $u_\theta = U_0$ on

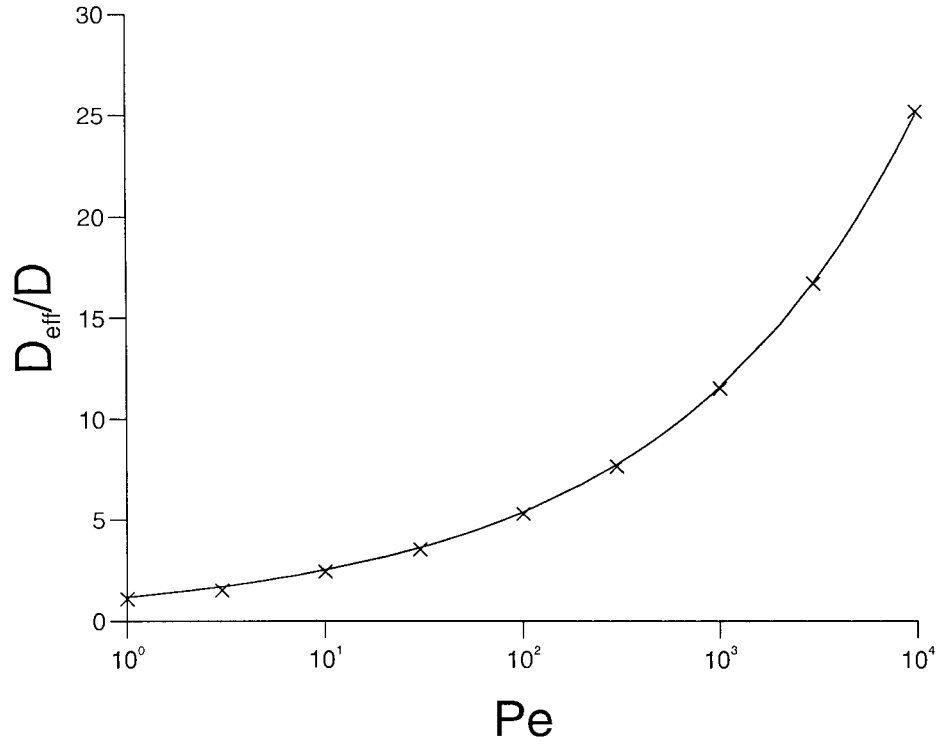

Figure 4. Comparison of the analytical prediction (continuous line) given by Equation (21) with the numerical solution ($\times$) of the effective diffusivity D_{eff}/D as a function of Pe.

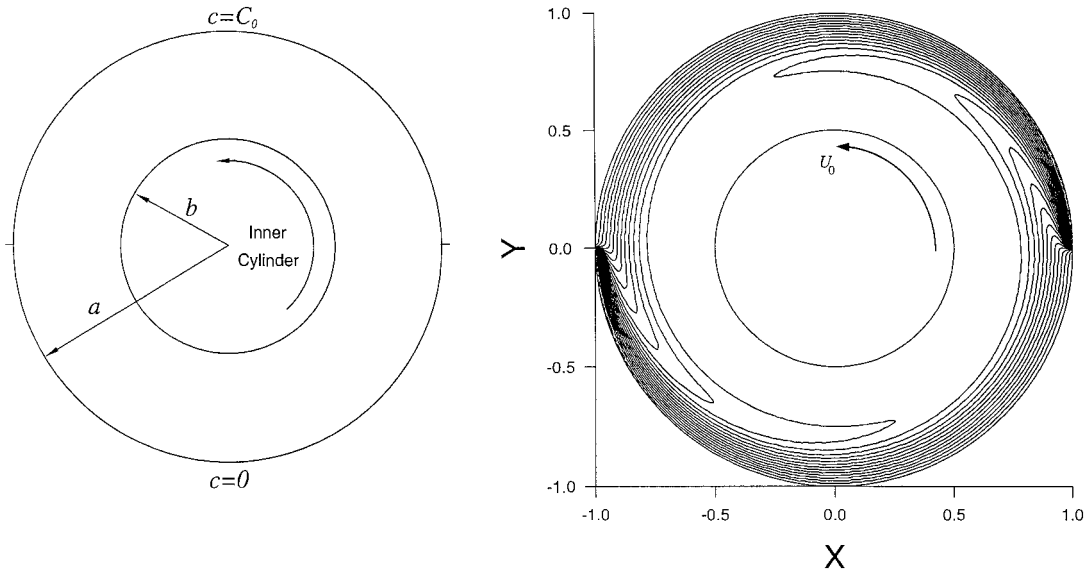

Figure 5. (a) Sketch of the two concentric-cylinders-model problem. The flow is generated by the counterclockwise rotation of the inner cylinder; (b) Concentration contours in the region between the two concentric cylinders obtained from a numerical solution of the full transport equation for $\text{Pe}\phi = 10^3$ with $\kappa = \frac{1}{2}$.

$r = b$, where u_θ and u_r are the θ and r-velocity components with respect to the cylindrical coordinate system (r, θ), whose origin is placed at the centre of the cylinders, as illustrated in Figure 5a. The fluid flow is a simple (anti-clockwise) rotation given by

$$u_\theta = \frac{U_0 b}{a^2 - b^2}\left(\frac{a^2}{r} - r\right), \quad u_r = 0 \tag{22}$$

which satisfies both the continuity and Navier-Stokes equations.

We now introduce a passive species into the fluid with a concentration $c = C_0$ at $r = a$ for $0 < \theta \leq \pi$. We also impose a macroscopic gradient by which the absorbed species is removed completely from the system such that $c = 0$ at $r = a$ for $\pi < \theta \leq 2\pi$. The inner cylinder is taken to be impermeable and so a no-flux boundary condition is imposed: $c_r = 0$ at $r = b$.

The steady-state mass transport satisfies $(\mathbf{u} \cdot \nabla)c = D\nabla^2 c$ which in cylindrical coordinates becomes, in dimensionless form,

$$\mathrm{Pe}\phi(1 - R^2)C_\tau = R^2 C_{RR} + RC_R + \pi^{-2} C_{\tau\tau} \tag{23a}$$

where $c = C_0 C$, $r = aR$ and $\theta = \pi\tau$, with $\mathrm{Pe} = U_0(a - b)/D$ now being the Péclet number and $\phi = \kappa/(1 - \kappa)^2(1 + \kappa)\pi$ a dimensionless parameter expressing the relative importance of the ratio $\kappa = b/a$. The boundary conditions are

$$C_R = 0 \quad \text{at} \quad R = \kappa, \tag{23b}$$

$$C = 1 \quad \text{at} \quad R = 1 \quad \text{for} \quad 0 < \tau \leq 1, \tag{23c}$$

$$C = 0 \quad \text{at} \quad R = 1 \quad \text{for} \quad 1 < \tau \leq 2. \tag{23d}$$

Figure 5b depicts a typical concentration field obtained from a numerical solution of (23).

3.1. Boundary-layer analysis, $\mathrm{Pe} \gg 1$

An analysis similar to that given for the cavity case (see Section 2) shows the existence of a concentration boundary layer of thickness $\delta \sim \mathrm{Pe}^{-1/3}$ present near the stationary outer cylinder and a homogeneous concentration outer region, to leading order (the size of this region will increase as Pe increases). We assume that the dimensionless boundary-layer thickness is much smaller than the dimensionless distance between the cylinders, *i.e.* $(2\phi\mathrm{Pe})^{-1/3} \ll 1 - \kappa$, or $\mathrm{Pe} \gg (1 + \kappa)\pi/2(1 - \kappa)$.

Using the same arguments with the cavity problem, we can easily demonstrate that $C(R, \tau) = 1 - C(R, 1 + \tau)$ and hence only the solution for $0 < \theta \leq \pi$ is required. Furthermore, the value of the concentration in the spatially homogeneous outer region is $1/2$. We now substitute the boundary-layer coordinate $\sigma = (2\phi\mathrm{Pe})^{1/3}(1 - R)$ in the mass-transport Equation (23a) which results in

$$\left(\sigma(2\phi\mathrm{Pe})^{\frac{2}{3}} - 2^{-\frac{2}{3}}\sigma^2(2\phi\mathrm{Pe})^{\frac{1}{3}}\right)C_\tau = \left((2\phi\mathrm{Pe})^{\frac{1}{3}} - \sigma\right)^2 C_{\sigma\sigma} - \left((2\phi\mathrm{Pe})^{\frac{1}{3}} - \sigma\right)C_\sigma + \pi^{-2} C_{\tau\tau}.$$

Retaining only the leading-order terms, we have

$$\sigma C_\tau = C_{\sigma\sigma} + O(\mathrm{Pe}^{-1/3}) \tag{24}$$

the solution of which must satisfy the boundary conditions

$$C = h(\sigma) \quad \text{at} \quad \tau = 0, \quad C \to \tfrac{1}{2} \quad \text{as} \quad \sigma \to \infty \quad \text{and} \quad C = 1 \quad \text{at} \quad \sigma = 0 \tag{25}$$

for $0 < \tau \leq 1$. The unknown function $h(\sigma)$, the concentration C on $\tau = 0$, will be determined from a global self-consistency condition.

3.2. Solution for the inner region

The analysis is identical to that for the wall AB of the stationary cavity problem and therefore the concentration in the upper boundary layer is given by

$$C = 1 - \frac{3^{\frac{1}{3}}}{2\Gamma(\frac{1}{3})} \int_0^{\sigma/\tau^{\frac{1}{3}}} \mathrm{e}^{-z^3/9} dz + \frac{3}{4} \int_0^{\infty} z\mathrm{e}^{-z^3\tau} G(-z\sigma) \int_0^{\infty} \left(h(p) - \tfrac{1}{2}\right) pG(-zp) \mathrm{d}p \, \mathrm{d}z. \tag{26}$$

Simple symmetry considerations now indicate that $C(\sigma, 0) = 1 - C(\sigma, 1)$, and hence

$$h(\sigma) = H(\sigma) - \frac{3}{4} \int_0^{\infty} z\mathrm{e}^{-z^3} G(-z\sigma) \int_0^{\infty} \left(h(p) - \tfrac{1}{2}\right) pG(-zp) \mathrm{d}p \, \mathrm{d}z, \tag{27}$$

where $H(\sigma)$ is the function introduced in Equation (16). Equation (27) is our global self-consistency condition. Unlike the stationary cavity problem, where the global condition (20) had to be solved numerically, an analytical solution of integral Equation (27) is possible.

For this purpose, let $f(\sigma) = h(\sigma) - \frac{1}{2}$ and $g(\sigma) = H(\sigma) - \frac{1}{2}$. The Airy transforms of these functions are $P(y) = \frac{\sqrt{3}}{2} \int_0^{\infty} f(x) x G(-xy) dx$ and $Q(y) = \frac{\sqrt{3}}{2} \int_0^{\infty} g(x) x G(-xy) dx$ and hence $f(x) = \frac{\sqrt{3}}{2} \int_0^{\infty} P(y) y G(-xy) dy$ and $g(x) = \frac{\sqrt{3}}{2} \int_0^{\infty} Q(y) y G(-xy) dy$. Equation (27) can now be written as

$$f(\sigma) = g(\sigma) - \frac{3}{4} \int_0^{\infty} z\mathrm{e}^{-z^3} G(-z\sigma) \int_0^{\infty} f(p) pG(-zp) \mathrm{d}p \, \mathrm{d}z,$$

which, after using the definition of the transform of f, yields

$$\frac{\sqrt{3}}{2} \int_0^{\infty} z(1 + \mathrm{e}^{-z^3}) G(-z\sigma) P(z) \mathrm{d}z = g(\sigma).$$

Taking the transform of this equation, we have

$$(1 + \mathrm{e}^{-z^3}) P(z) = Q(z). \tag{28}$$

Rearranging for P and taking the transform of the new equation allows us to obtain

$$f(\sigma) = \frac{\sqrt{3}}{2} \int_0^{\infty} (1 + \mathrm{e}^{-z^3})^{-1} Q(z) z G(-z\sigma) \mathrm{d}z$$

and thus f can be expressed as a double integral that involves g, namely

$$f(\sigma) = \frac{3}{4} \int_0^{\infty} (1 + \mathrm{e}^{-z^3})^{-1} z G(-z\sigma) \int_0^{\infty} pG(-pz) g(p) \mathrm{d}p \, \mathrm{d}z.$$

Therefore,

$$h(\sigma) = \frac{1}{2} + \frac{3}{4} \int_0^{\infty} (1 + \mathrm{e}^{-z^3})^{-1} z G(-z\sigma) \int_0^{\infty} pG(-pz) \left(H(p) - \tfrac{1}{2}\right) \mathrm{d}p \, \mathrm{d}z \tag{29}$$

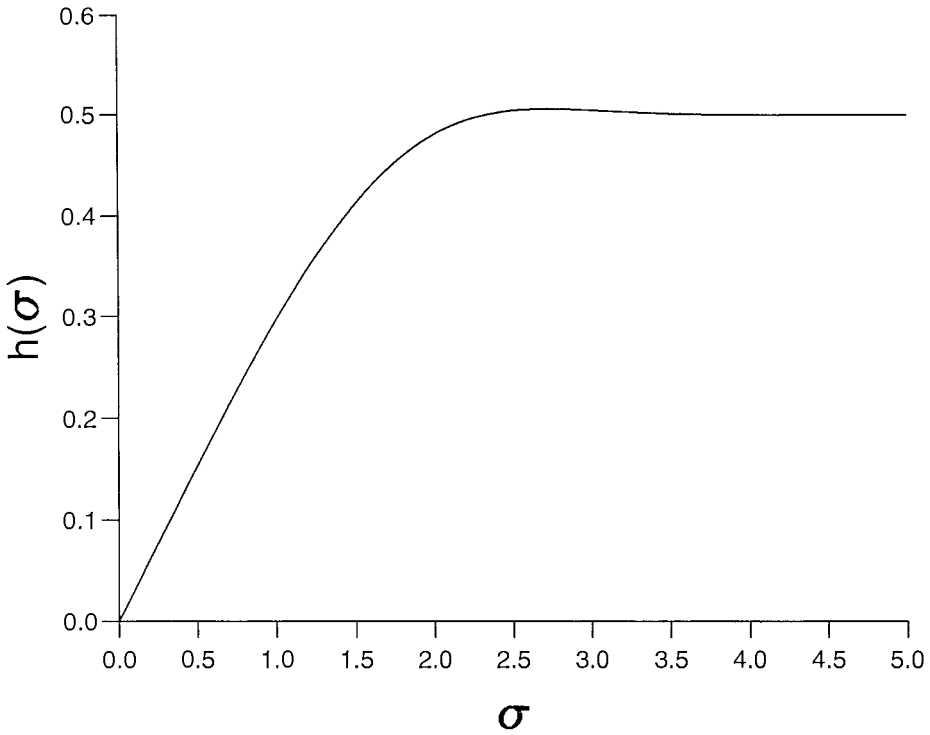

Figure 6. The concentration $h(\sigma)$, given by expression (29), near $\tau = 0$.

and C can now be obtained from (26).

The function $h(\sigma)$ was evaluated by numerical integration – see Figure 6 – with the same criteria as before on domain size and step size to insure that sufficiently accurate results were obtained – a domain size of 20 with uniform step sizes of 0·004 was used. We notice that $h(\sigma) \to 0$ as $\sigma \to 0$ and $h(\sigma) \to 1/2$ as $\sigma \to \infty$. Again we see the classical overshoot around $\sigma = 2{\cdot}6$, which is followed by very rapidly decaying oscillations tending to a value of $1/2$ into the outer region (not visible in the graph).

Figure (7a) depicts the inner region concentration contours in (σ, τ) co-ordinates obtained from the boundary-layer analysis. Notice the excellent agreement with the numerical solution of the full transport Equation (23a) shown in Figure (7b) for $\mathrm{Pe}\phi = 10^3$ and $\kappa = \frac{1}{2}$. The numerical solution was determined by means of a standard finite-difference method in polar co-ordinates $r - \theta$, with the solution then mapped onto the $\sigma - \tau$ plane.

3.3. Effective diffusivity

Following Section 2.3, the effective diffusivity for the cylinders model is defined as

$$D_{\mathrm{eff}} = -\frac{fa}{C_0} = \frac{Da}{C_0\pi}\int_0^{\pi} c_r|_{r=a}\mathrm{d}\theta = D\int_0^1 C_R|_{R=1}\mathrm{d}\tau,$$

where f is the dimensional flux through the top surface. We now have, $\int_0^1 C_R|_{R=1}\mathrm{d}\tau = -(2\phi\mathrm{Pe})^{1/3}\int_0^1 C_\sigma|_{\sigma=0}\mathrm{d}\tau$, which can be obtained from (26) as

$$\int_0^1 C_\sigma|_{\sigma=0}\mathrm{d}\tau = -\frac{3^{4/3}}{4\Gamma(\frac{1}{3})} - \frac{3^{7/6}}{2\Gamma(\frac{1}{3})}\int_0^{\infty}\frac{1}{z}(1-\mathrm{e}^{-z^3})\int_0^{\infty}\left(h(p)-\tfrac{1}{2}\right)pG(-zp)\mathrm{d}p\,\mathrm{d}z.$$

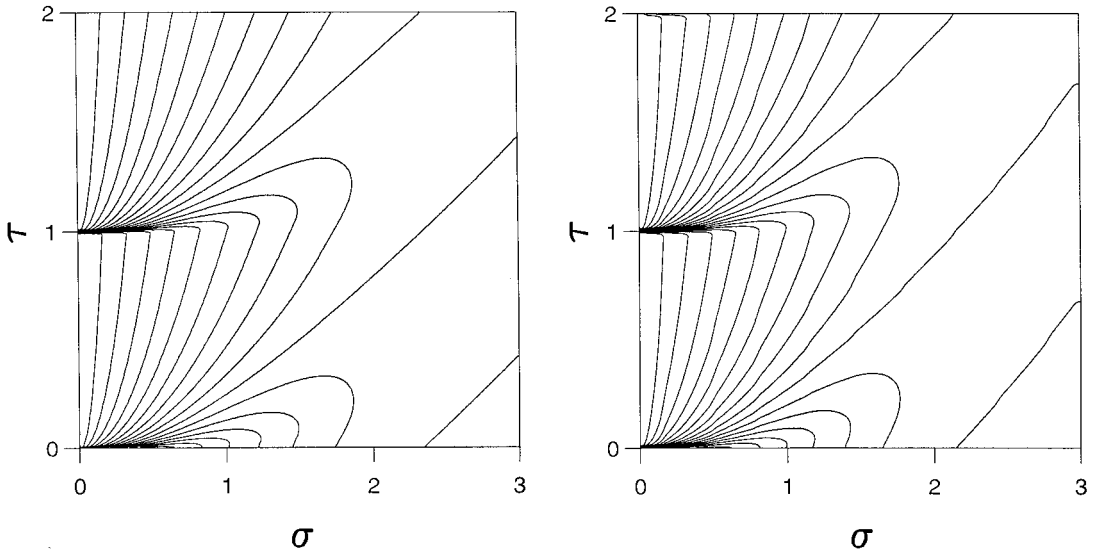

Figure 7. (a) Inner region concentration contours obtained from the boundary-layer solution; (b) Inner region concentration contours obtained numerically from the full transport equation (23*a*) for $\mathrm{Pe}\phi = 10^3$, $\kappa = \frac{1}{2}$ and mapped onto the $\sigma - \tau$ plane.

From Equation (28) we have

$$\int_0^1 C_\sigma|_{\sigma=0}\mathrm{d}\tau = -\frac{3^{4/3}}{4\Gamma(\frac{1}{3})} - \frac{3^{7/6}}{2\Gamma(\frac{1}{3})}\int_0^\infty \frac{(1-\mathrm{e}^{-z^3})}{z(1+\mathrm{e}^{-z^3})}\int_0^\infty \left(H(p)-\tfrac{1}{2}\right) pG(-zp)\mathrm{d}p\,\mathrm{d}z$$
$$= -0{\cdot}5450$$

The effective diffusivity is then given by

$$D_{\mathrm{eff}} = 0{\cdot}6741 D\phi^{1/3}\mathrm{Pe}^{1/3}. \tag{30}$$

This equation applies to both mass and heat transport with D_{eff}/D equivalent to the (mean) Nusselt number in the case of heat transport. A plot of D_{eff}/D obtained from (30) (full line) for $\kappa = 1/2$ is shown in Figure 8. Also shown are values obtained from a numerical solution of (23) over a range of Pe (shown by $\times$) for $\kappa = 1/2$. There is good agreement between the two sets of results even when Pe is $O(1)$, though the agreement is not quite as good as for the cavity problem (see Figure 4). We finally notice that, unlike (21) for the cavity problem, Equation (30) is valid for any ratio $\kappa = b/a$ provided, of course, $\mathrm{Pe} \gg (1+\kappa)\pi/2(1-\kappa)$ (see Section 3.1).

4. Conclusion

Mass-transport enhancement in regions bounded by mobile interfaces has been a subject of intense investigation over the years. In this paper, we have examined analytically the mechanism of mass-transport enhancement into a fluid bounded by rigid walls. Two problems were considered: a stationary cavity, where the flow field is induced by a disturbance located at the centre of the cavity, and a concentric-cylinders model, where the flow is induced by the rotation of the inner cylinder in its own plane. We analyzed the transport process in the large-Péclet-number limit using matched asymptotic expansions.

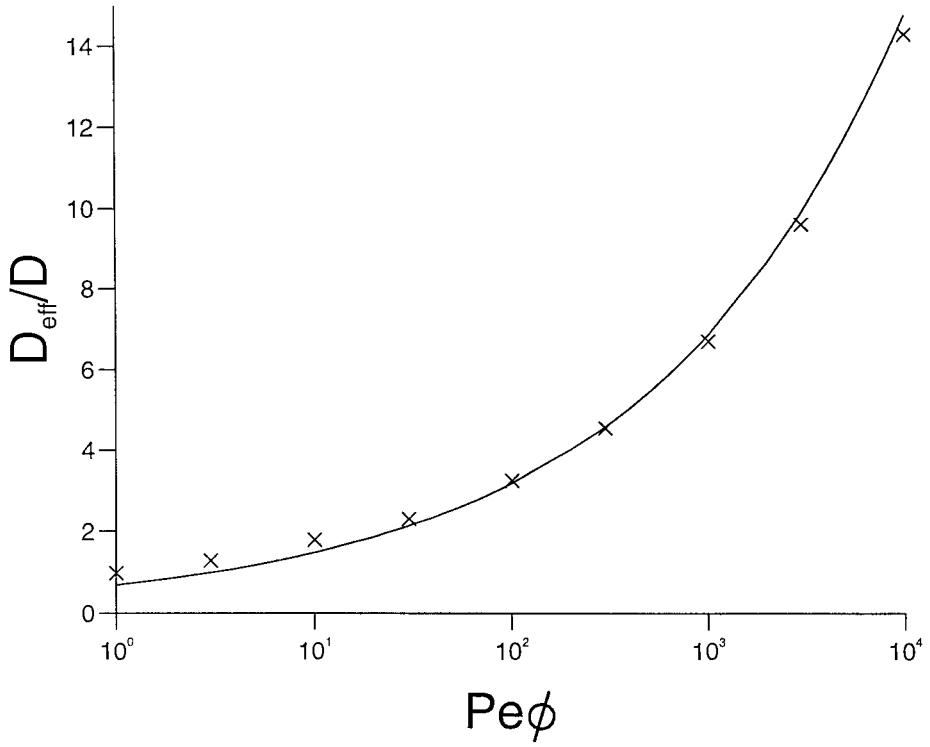

Figure 8. Comparison of the analytical prediction (continuous line) given by Equation (30) with the numerical solution ($\times$) of the effective diffusivity D_{eff}/D as a function of Pe and ϕ, with $\kappa = \frac{1}{2}$.

We have demonstrated that, when a macroscopic gradient is imposed, the primary mechanism for mass-transport is a large recirculation zone within the fluid, except close to the walls, where molecular diffusion balances convection in thin boundary layers. The enhancement over pure diffusion is found to scale as $\text{Pe}^{1/3}$. The method of calculation of the effective diffusivity can be easily generalized to describe flow-assisted diffusion in more general fluid flow structures.

Finally, there are a number of interesting questions related to the analysis presented here. For example, it would be interesting to compute the effective diffusivity in the presence of (slow) oscillatory convection. Another related problem would be the presence of active impurities in the flow, *i.e.* the case where the effect of varying concentration on the flow through buoyancy cannot be neglected (as is the case with binary convection).

Acknowledgements

We acknowledge financial support from the Engineering and Physical Sciences Research Council through grant no. GR/M73767.

Appendix 1. The Airy transform

The solutions of the equation $F'' - xF = 0$ are Airy functions [16, pp. 446–450], namely $\text{Ai}(x) = c_1 f(x) - c_2 g(x)$ and $\text{Bi}(x) = \sqrt{3}(c_1 f(x) + c_2 g(x))$, where

$$c_1 = \frac{3^{-\frac{2}{3}}}{\Gamma\left(\frac{2}{3}\right)}, c_2 = \frac{3^{-\frac{1}{3}}}{\Gamma\left(\frac{1}{3}\right)}, \text{ and } f(x) = \sum_{k=0}^{\infty} 3^k \left(\frac{1}{3}\right)_k \frac{x^{3k}}{(3k)!}, g(x) = \sum_{k=0}^{\infty} 3^k \left(\frac{2}{3}\right)_k \frac{x^{3k+1}}{(3k+1)!}.$$

Here $(m)_k = \prod_{n=0}^{k-1}(n+m)$ and $(m)_0 = 1$. The asymptotic behaviour of the Airy functions is $\mathrm{Ai}(-x) \simeq \pi^{-\frac{1}{2}} x^{-\frac{1}{4}} \sin(\frac{2}{3}x^{\frac{3}{2}} + \frac{\pi}{4})$ and $\mathrm{Bi}(-x) \simeq \pi^{-\frac{1}{2}} x^{-\frac{1}{4}} \cos(\frac{2}{3}x^{\frac{3}{2}} + \frac{\pi}{4})$ as $x \to \infty$.

Consider $Y'' + \lambda x Y = 0$ $(*)$ on $[0, L]$ with $Y(0) = 0$ and $Y(L) = 0$; then from standard Sturm-Liouville Theory there exists an infinite sequence $\{\lambda_n\}$ of real positive distinct eigenvalues with corresponding orthogonal eigenfunctions $\{Y_n\}$, satisfying $\int_0^L x Y_n^2 \mathrm{d}x = 1$. Further, any twice continuously differentiable function $j(x) : [0, L] \to \mathbb{R}$ satisfying $j(0) = j(L) = 0$ can be expanded in a uniformly convergent series of eigenfunctions, $j(x) = \sum_{n=1}^{\infty} c_n Y_n(x)$ where $c_n = \int_0^L j(x) x Y_n(x) \mathrm{d}x$.

Two linearly independent solutions of $(*)$ are $\mathrm{Ai}(-\lambda_n^{1/3}x)$ and $\mathrm{Bi}(-\lambda_n^{1/3}x)$, hence, $Y_n(x) = \alpha_n \mathrm{Ai}(-\lambda_n^{1/3}x) + \beta_n \mathrm{Bi}(-\lambda_n^{1/3}x)$. Now $Y_n(0) = 0$ gives $\alpha_n + \beta_n\sqrt{3} = 0$ and $Y_n(L) = 0$ gives $\sqrt{3}\mathrm{Ai}(-\lambda_n^{1/3}L) = \mathrm{Bi}(-\lambda_n^{1/3}L)$, which after using the asymptotic approximations results in $\tan\left(\frac{2}{3}\lambda_n^{1/2}L^{3/2} + \frac{\pi}{4}\right) \simeq \frac{1}{\sqrt{3}}$, thus, $\lambda_n \simeq \left(3\pi(n - \frac{1}{12})L^{-3/2}/2\right)^2$ with $\Delta\lambda^{1/2} \simeq 3\pi L^{-3/2}/2$, for large n, where $\Delta\lambda^{1/2} = \lambda_{n+1}^{1/2} - \lambda_n^{1/2}$.

Introducing $G(z) = -\sqrt{3}\mathrm{Ai}(z) + \mathrm{Bi}(z)$, we have $Y_n(x) = \beta_n G(-\lambda_n^{1/3}x)$ and from Appendix 2, the normalisation coefficient $\beta_n \simeq \lambda_n^{1/12}(\Delta\lambda^{1/2})^{1/2}/\sqrt{2}$. Hence, using the eigenfunction expansion, $j(x) = \sum_{n=1}^{\infty} Y_n(x) \int_0^L j(p) p Y_n(p)\, \mathrm{d}p$, we have

$$j(x) = \frac{1}{2}\sum_{n=1}^{\infty} \lambda_n^{1/6} G(-\lambda_n^{1/3}x)(\Delta\lambda^{1/2}) \int_0^L j(p) p G(-\lambda_n^{1/3}p)\, \mathrm{d}p$$

Similarly the function $\overline{G}(z)$ (first introduced in (17)) which satisfies $\overline{G}_z(0) = 0$ instead of $G(0) = 0$ has $\lambda_n \simeq (3(n - \frac{5}{12})\pi/2L^{3/2})^2$ with the same β_n.

We now let $L \to \infty$, as our inner region is defined in an infinite domain, and after substituting $z = \lambda_n^{1/3}$, we arrive at

$$j(x) = \frac{3}{4}\int_0^{\infty} z G(-zx) \int_0^{\infty} j(p) p G(-zp) \mathrm{d}p\, \mathrm{d}z$$

for any smooth function $j(x)$ which decays faster than $x^{-3/4}$ as $x \to \infty$. This leads us to define the *Airy transform*

$$A[j(x)] = J(y) = \frac{\sqrt{3}}{2}\int_0^{\infty} j(x) x G(-xy)\, \mathrm{d}x$$

with inverse

$$A^{-1}[J(y)] = j(x) = \frac{\sqrt{3}}{2}\int_0^{\infty} J(y) y G(-xy)\, \mathrm{d}y.$$

Appendix 2: The normalisation coefficient

Defining $u(x) = G(-\lambda^{1/3}x)$ and $v(x) = G(-\lambda_n^{1/3}x)$ such that $u_{xx} + \lambda xu = 0$ and $v_{xx} + \lambda_n xv = 0$, where $u(0) = v(0) = 0$ and $v(L) = 0$. Then $v(u_{xx} + \lambda_n xu) - u(v_{xx} + \lambda xv) = 0$ which after integrating over the domain $[0, L]$ gives

$$(\lambda - \lambda_n)\int_0^L xuv\mathrm{d}x = u(L)v_x(L)$$

and hence

$$\int_0^L xG(-\lambda^{1/3}x)G(-\lambda_n^{1/3}x)\mathrm{d}x = \frac{G(-\lambda^{1/3}L)G_x(-\lambda_n^{1/3}x)|_{x=L}}{\lambda - \lambda_n}.$$

Now,

$$\begin{aligned}\int_0^L x(G(-\lambda_n^{1/3}x))^2\mathrm{d}x &= \lim_{\lambda\to\lambda_n}\int_0^L xG(-\lambda^{1/3}x)G(-\lambda_n^{1/3}x)\mathrm{d}x\\ &= \lim_{\lambda\to\lambda_n}\frac{G(-\lambda^{1/3}L)G_L(-\lambda_n^{1/3}L)}{\lambda - \lambda_n}\\ &= \frac{1}{3}L\lambda_n^{-1/3}G_z(-z)^2|_{z=\lambda_n^{1/3}L}\end{aligned}$$

using L'Hôpital's rule. The asymptotic approximations for the Airy functions, results in $G_z(-z) \simeq (-1)^n 2\pi^{-1/2}\lambda_n^{1/12}L^{1/4}$. Hence,

$$\int_0^L x(G(-\lambda_n^{1/3}x))^2\mathrm{d}x \simeq \tfrac{4}{3}\lambda_n^{-1/6}L^{3/2}\pi^{-1} = 2\lambda_n^{-1/6}(\Delta\lambda^{1/2})^{-1}.$$

Since $1 = \int_0^L xY_n^2\mathrm{d}x = \beta_n^2\int_0^L x(G(-\lambda_n^{1/3}x))^2\mathrm{d}x$, hence $\beta_n \simeq \lambda_n^{1/12}(\Delta\lambda^{1/2})^{1/2}/\sqrt{2}$.

References

1. S.L. Goren and P.V.S. Mani, Mass transfer through horizontal liquid films in wavy motion. *AIChE J.* 14 (1968) 57–61.
2. R.M. Roberts and H.-C. Chang, Wave-enhanced interfacial transfer. *Chem. Eng. Sci.* 55 (2000) 1127–1141.
3. H. Aref and S. Balachandar, Chaotic advection in a Stokes flow. *Phys. Fluids* 29 (1986) 3515–3521.
4. J. Chaiken, R. Chevray, M. Tabor and Q.M. Tam, Experimental study of Lagrangian turbulence in Stokes flow. *Proc. R. Soc. London A* 408 (1986) 165–174.
5. J.M. Ottino, *The Kinematics of Mixing: Stretching, Chaos and Transport*. Cambridge University Press, Cambridge (1989) 364 pp.
6. S. Ghosh, H.-C. Chang and M. Sen, Heat-transfer enhancement due to slender recirculation and chaotic transport between counter-rotating eccentric cylinders. *J. Fluid Mech.* 238 (1992) 119–154.
7. G. Baier, M.D. Graham and E.N. Lightfoot, Mass transport in a novel two-fluid Taylor vortex extractor. *AIChE J.* 46 (2000) 2395–2405.
8. P.M.J. Trevelyan, S. Kalliadasis, J.H. Merkin and S.K. Scott, Circulation and reaction enhancement of mass-transport in a cavity, *Chem. Eng. Sci.* (2001) to appear.
9. J. Patterson and J. Imberger, Unsteady natural convection in a rectangular cavity. *J. Fluid Mech.* 100 (1980) 65–86.
10. B.I. Shraiman, Diffusive transport in a Rayleigh-Bénard convection cell. *Phys. Rev. A* 36 (1987) 261–267.
11. A.D. Polyanin, Some qualitative features of (internal) problems of heat and mass transfer in regions with closed streamlines. *Izvestiya Akademii Nauk SSSR* 5 (1983) 116–125.

12. W. Young, A. Pumir and Y. Pomeau, Anomalous diffusion of tracer in convection rolls. *Phys. Fluids* 3 (1989) 462–469.
13. M.N. Rosenbluth, H.L. Berk, I. Doxas and W. Horton, Effective diffusion in laminar convective flows. *Phys. Fluids* 30 (1987) 2636–2647.
14. W.E. Stewart, *Physicochemical Hydrodynamics*. V.G. Levich Festschrift. Spalding (1977) 1076 pp.
15. A. Acrivos and J.D. Goddard, Asymptotic expansions of laminar forced-convection heat and mass transfer. Part 1. Low speed flows. *J. Fluid Mech.* 23 (1965) 273–291.
16. M. Abramowitz and I.A. Stegun, *Handbook of Mathematical Functions*. Dover (1970) 1046 pp.
17. H.K. Kuiken, Heat or mass transfer from an open cavity. *J. Eng. Math.* 12 (1978) 129–155.